Motion-Guided Segmentation for Cine DENSE MRI

Bruce S. Spottiswoode[1], **Xiaodong Zhong**[2], **Christine H. Lorenz**[3], **Bongani M. Mayosi**[4], **Ernesta M. Meintjes**[1], and **Frederick H. Epstein**[5]

1 *UCT/MRC Medical Imaging Research Unit, University of Cape Town, South Africa*

2 *Department of Biomedical Engineering, University of Virginia, Virginia, United States*

3 *Siemens Medical Solutions, Baltimore, Maryland, United States*

4 *Cardiac Clinic at Groote Schuur Hospital and the Department of Medicine, University of Cape Town, South Africa*

5 *Departments of Radiology and Biomedical Engineering, University of Virginia, Virginia, United States*

Abstract

Defining myocardial contours is often the most time consuming portion of dynamic cardiac MRI image analysis. Displacement encoding with stimulated echoes (DENSE) is a quantitative MRI technique that encodes tissue displacement into the phase of the complex MRI images. Cine DENSE provides a time series of these images, thus facilitating the non-invasive study of myocardial kinematics. Epicardial and endocardial contours need to be defined at each frame on cine DENSE images for the quantification of regional displacement and strain as a function of time. This work presents a reliable and effective two dimensional semi-automated segmentation technique that uses the encoded motion to project a manually defined region of interest through time. Contours can then easily be extracted for each cardiac phase. This method boasts several advantages, including, 1. parameters are based on practical physiological limits, 2. contours are calculated for the first few cardiac phases, where it is difficult to visually distinguish blood from myocardium, and 3. the method is independent of the shape of the tissue delineated and can be applied to short- or long-axis views, and on arbitrary regions of interest. Motion-guided contours were compared to manual contours for six conventional and six slice-followed mid-ventricular short-axis cine DENSE datasets. Using an area measure of segmentation error, the accuracy of the segmentation algorithm was shown to be similar to inter-observer variability. In addition, a radial segmentation error metric was introduced for short-axis data. The average radial epicardial segmentation error was 0.36±0.08 and 0.40±0.10 pixels for slice followed and conventional cine DENSE, respectively, and the average radial endocardial segmentation error was 0.46±0.12 and 0.46±0.16 pixels for slice following and conventional cine DENSE, respectively. Motion-guided segmentation employs the displacement-encoded phase shifts intrinsic to DENSE MRI to accurately propagate a single set of pre-defined contours throughout the remaining cardiac phases.

Keywords

Cardiac MRI; DENSE; myocardial tagging; segmentation; tissue tracking

1 INTRODUCTION

A number of MRI techniques have been developed to quantify myocardial motion, including myocardial tagging (Zerhouni et al., 1988; Axel and Dougherty, 1989), phase contrast (PC) velocity encoding (van Dijk, 1984; Bryant et al., 1984), and more recently, displacement encoding with stimulated echoes (DENSE) (Aletras et al., 1999). DENSE has the advantage over velocity-encoded PC of directly measuring tissue displacement instead of velocity, and the advantages over tagging of higher spatial resolution and more direct computation of displacement. Quantitative methods are potentially useful for reducing subjectivity and improving accuracy (Gotte et al., 2001) in the clinical assessment of cardiac wall motion, but their clinical use is currently limited by lack of automation.

Defining epicardial and endocardial contours is an integral step in quantifying regional cardiac wall motion. For cine DENSE (Kim et al., 2004) these contours are typically manually delineated for all cardiac phases, which is a laborious process and is currently the most time-consuming component of the cine-DENSE image analysis. Automated myocardial contour detection techniques based on image intensity may not be well-suited to cine DENSE because: 1. boundaries between the myocardium and adjacent tissue (e.g. the liver) are often indiscernible based on signal magnitude; 2. a T1-related decay in signal-to-noise ratio (SNR) with time is often present; and 3. high signal is present in the blood pool of the first few frames, before it is washed out of the image plane.

A number of advances have been made towards automating image segmentation for myocardial tagging and velocity encoding (Kumar and Goldgof, 1994; Young et al., 1995; Kraichman et al., 1995; Guttman et al., 1994; Montillo et al., 2002; Montillo et al., 2003; Wong et al., 2002; Cho and Benkeser, 2006) but no segmentation algorithm specifically tailored for cine DENSE has been developed. A segmentation method is presented here that uses tissue tracking based on the motion encoded into the phase of the cine DENSE images themselves to project individual manually-defined contours through time. The method is shown to be accurate, versatile and practical, and forms a significant step towards the automation of cine DENSE image analysis.

2 Cine DENSE MRI and Tissue Tracking

DENSE uses the phase of the stimulated echo to monitor myocardial motion and deformation at a pixel resolution. The magnetization is initially position encoded using two 90° radiofrequency pulses separated by a gradient pulse, which are typically applied at end-diastole. Tissue displacement that occurs between the displacement-encoding pulses and subsequent data acquisition times causes a phase shift of the stimulated echo, resulting in images with pixel phase proportional to tissue displacement. Cine DENSE provides a time series of such displacement measurements.

Cine DENSE allows for displacement encoding in any direction, but 2 or 3 orthogonal directions are typically inferred. These directions can either be encoded directly or derived using a balanced multi-point encoding strategy (Zhong et al., 2007:1). Since only the final phase accrual of the signal is measured, the measured phase is inherently confined to the range $-\pi < \phi < \pi$. The true phase is thus wrapped to lie within this range, and spatiotemporal phase unwrapping is required for absolute displacement measurements (Spottiswoode et al., 2007).

Fig 1(a) shows a cine DENSE magnitude-reconstructed image of a mid-ventricular short-axis view of the heart. The left and right ventricles are shown, as are the epicardial and endocardial borders of the left ventricle (LV). It is these contours at all cardiac phases that are typically sought after for LV analysis in short-axis images. Fig 1(b) shows the corresponding 2D displacement field derived from phase-unwrapped cine DENSE images encoded for 2D in-

plane motion. DENSE displacement vectors are visualized as having heads positioned at the centre of all myocardial pixels, and tails originating from the reference position of these pixels at the time of displacement encoding, t_0.

As the heart deforms, a material point moves from its reference point $\mathbf{p}=(p1, p2)$ at time t_0 to a new spatial position $\mathbf{x}$ at time frame t_n. Here $t_n = t_1, \ldots, t_F$, where F is the number of frames in the series, and t_0 is the time of displacement encoding. The reference map $\mathbf{p}(\mathbf{x}, t_n)$ characterizes this motion, where $\mathbf{p}(\mathbf{x}, t_0)=\mathbf{p}$. If displacement is encoded in two orthogonal directions $\hat{\mathbf{i}}$ and $\hat{\mathbf{j}}$, then the 2D DENSE displacement field can be calculated, and is given by $\mathbf{u}(\mathbf{x}, t_n)=\mathbf{p}(\mathbf{x}, t_n)-\mathbf{p}$. Note that the time between t_0 and t_1 is usually around 3 ms, and corresponds to the time between displacement encoding and the first cardiac phase imaged. This is much shorter than the uniform time intervals $t_2 - t_1, \ldots, t_F - t_{F-1}$.

Two-dimensional frame-to-frame motion trajectories for discrete elements of the myocardium can be obtained using 2D distance weighted linear interpolation of these displacement vectors (Spottiswoode et al., 2007). This tracking method is demonstrated for a single frame-to-frame trajectory in Fig 2. Fig 2(a) shows a DENSE displacement field of the LV at end-systole, and Fig 2(b) is an isolated portion of this image. All solid vectors have heads at pixel centers. The tail of the dotted (purple) vector depicts an arbitrarily chosen starting point at t_0. For each frame $t_1, \ldots, t_F$, the three vector tails closest to this starting position are identified. These are shown as solid dark (red) vectors in Fig 2(b) for the end-systolic frame. Two dimensional distance-weighted linear interpolation yields the position of this starting point at each frame (dotted vector in Fig 2(b)). Fig 2(c) shows the frame-to-frame trajectory obtained by subtracting the interpolated vectors of successive frames from each other. Trajectories can be improved by fitting 5th order periodic Fourier basis functions to each of the $\hat{\mathbf{i}}$ and $\hat{\mathbf{j}}$ components of motion as a function of time (Spottiswoode *et al.*, 2007). Fig 2(d) shows the fitted version of the trajectory shown in Fig 2(c),

3 METHODS

We propose using the motion encoded within the cine DENSE images to guide the segmentation process. This is achieved by using the myocardial motion trajectories to project any manually defined portion of myocardium at one cardiac phase onto all other cardiac phases. Since the cine DENSE displacement fields all reference time t_0, the initial contour(s) can be drawn on any cardiac phase. The displacement vector starting points of every pixel in the manually contoured region thus define the position of the selected portion of myocardium at t_0, and tracking these starting points though time identifies the position of this myocardium at all other frames.

While the basic concept is straightforward, the implementation is complicated by the presence of phase noise. If spatiotemporal phase unwrapping is performed without pre-defined contours, then regions of noisy phase produce randomly scaled and oriented displacement vectors. An example of an un-contoured DENSE displacement field for the region portrayed in Fig 3(a) is shown in Fig 3(b). The phase data in the blood and pulmonary cavity has very low signal-to-noise ratio, and the appearance of these displacement vectors is essentially random. The smoothly varying motion in the LV is evident contracting towards the center of the image. The aim here is to extract only vectors in the myocardium from such displacement fields given a set of predefined myocardial starting points at t_0.

Obtaining suitable motion trajectories from noisy displacement fields requires a series of refinements to the motion tracking algorithm described above, where the 3 nearest vector tails are selected for 2D distance-weighted linear interpolation. If a manually-defined set of myocardial points at t_0 are tracked using this algorithm, then frame-to-frame trajectories such

as those shown in Fig 4(a) result. Many of these trajectories are incorrect because noisy vectors from the lungs and blood pools intrude into the myocardium and are inadvertently used for the 2D interpolations.

These trajectories can be improved by applying the following three steps:

1. Remove noisy displacement vectors using a modulus *deformation mask*, which is obtained for each frame t_n by combining orthogonal spatial derivatives of the displacement fields as follows:

$$M(\mathbf{x},t_n)=\frac{1}{2}\sum\nolimits_{k=\widehat{\mathbf{i}},\widehat{\mathbf{j}}}\left[\left(\frac{\partial u_k(\mathbf{x},t_n)}{\partial\widehat{\mathbf{i}}}\right)^2+\left(\frac{\partial u_k(\mathbf{x},t_n)}{\partial\widehat{\mathbf{j}}}\right)^2\right]^{1/2}$$

(1)

where $u_{\widehat{\mathbf{i}}}$ and $u_{\widehat{\mathbf{j}}}$ represent the components of the cine DENSE displacement field in the $\widehat{\mathbf{i}}$ and $\widehat{\mathbf{j}}$ directions, respectively, for spatial position $\mathbf{x}$ within the image plane. The deformation mask corresponding to Fig 3(b) is shown in Fig 3(c). By setting a threshold that excludes all deformation values greater than those found in the human heart, the majority of the noisy displacement vectors are eliminated. A magnitude deformation threshold of 70% was used here. The deformation mask can be related to standard measures of myocardial strain, and this threshold of 70% is well above typical strain values (Moore et al. 2000). Fig 4(b) shows the resulting trajectories if such a deformation mask is used prior to applying the tracking algorithm. These are less noisy than the trajectories shown in Fig 4(a).

2. For each frame, apply heuristic rules based on the behavior of displacement vectors in a local region to further eliminate/exclude noisy vectors in the tracking process. The deformation masks remove the majority of the noisy vectors and it is thus reasonable to eliminate remaining noisy vectors based on their deviation from the mean magnitude and angle of nearby vectors. The 9 vectors with tails nearest to each starting point at t_0 are selected, and vectors with an angle deviation greater than $\pi/6$ radians and a magnitude deviation greater than 0.7 are ignored. The remaining closest 3 vector tails are then used for tracking. The trajectories shown in Fig 4(c) portray the improvement offered by these rules. The reasoning behind these limiting values is as follows: For any starting point, the average distance to the 9 nearest vector tails will be equal to the spatial resolution. Although the implementation is different to the deformation mask, we apply the same rationale and base this on a maximum magnitude deviation of 0.7 between two points. The angle deviation threshold of $\pi/6$ radians is chosen based on our experience with cine DENSE displacement fields and is considerably higher than the angle deviation we have encountered even in infarct border zones where we expect the largest angle deviations. These limiting values of angle and magnitude deviation yield satisfactory results without limiting the expected range of myocardial motion.

3. Trajectories are further improved by applying temporal fitting as described in Spottiswoode et al. (2007). Periodic Fourier basis functions are fitted to each of the horizontal and vertical components of motion as a function of time. Fig 4(d) shows the result of this process where the remaining spikes in the trajectories have been removed.

Steps 1 and 2 serve to remove noise due to extramyocardial phase measurements randomly having displacement origins within the end-diastolic myocardium, whereas step 3 removes noise due to the finite cine DENSE SNR within the myocardium. Note also that the magnitude deviation, which is based on positions of vector tails, is a different measure than the deformation mask, which is computed at each pixel. The trajectories in Fig 4(d) give an indication of the position of the selected myocardium at each cardiac phase, and the remainder of the segmentation process involves extracting the epicardial and endocardial contours from this short-axis data. Once all of these contours have been extracted the displacement data can be

masked and the tracking can be redone commencing from the centers of a uniform grid at the first cardiac phase. These trajectories are shown in Fig 4(e) and can be used for analyzing myocardial strain as described in Spottiswoode et al. (2007).

If every trajectory position at a particular frame is represented at a sub-pixel resolution by a 2D Gaussian function with an area of unity, then an image such as Fig 5(a) results. Contours can then easily be extracted as isolines along an intensity level of 0.5. This process is repeated for all frames. For short-axis views the longest contour is defined as the epicardium and the second longest is defined as the endocardium. For reference, Fig 5(b) shows a binary mask of the myocardium which is obtained by dichotomizing the image in Fig 5(a) using a threshold of 0.5. A Gaussian standard deviation of 1.25 pixels was found to be suitable for this application, but this value would need modification in proportion to the tracking spatial resolution if this differs from the image spatial resolution. If the standard deviation is set too high or too low then islands of myocardium would typically occur, as illustrated in Fig 6.

Finally, the resulting contours are smoothed by fitting periodic curves to each of the spatial directions $\hat{\mathbf{i}}$ and $\hat{\mathbf{j}}$ as a function of arc length s. Fourier basis functions were used as follows

$$f_{\widehat{\mathbf{i}},\widehat{\mathbf{j}}}(s)=\frac{1}{2}a_0+\sum_{m=1}^{N}a_m\cos(m\omega s)+\sum_{m=1}^{N}b_m\sin(m\omega s)$$

(2)

where a_m and b_m are the Fourier series coefficients, $\omega = 2\pi/S$ is the spatial angular frequency, S is the total arc length of the contour, and N is the order of the fit. The arc length s is derived by summing the discrete lengths of the straight line segments along the isoline. Fitting was done using least squares and 4th order functions, requiring 18 coefficients for both directions, were found to be adequate to describe the short-axis contour shapes encountered in this study. The variation in contour shape from frame-to-frame is often small, so the processing time can be reduced by using the fitted Fourier coefficients for a particular frame as starting coefficients for an unfitted adjacent frame. A table with a list of all the free parameters used in the motion guided segmentation algorithm, as well as their effect on the algorithm and the selection criteria, is presented in the Appendix.

4 EXPERIMENT AND VALIDATION

The cine DENSE scans were performed on 1.5 T Siemens Sonata and Avanto scanners (Siemens Medical Systems, Erlangen, Germany). Six normal volunteers were scanned, and all subjects provided informed consent and were studied in accordance with research protocols approved by the Human Investigations Committee at the University of Virginia. Both conventional cine DENSE (Kim et al., 2004) and slice-followed cine DENSE (Spottiswoode et al., 2008) data were acquired for each volunteer, with displacement encoding applied in two orthogonal in-plane directions. Slice following (Fischer et al., 1994; Stuber et al., 1999) uses the subtraction of two different acquisitions with complementary slice-selective displacement encoding to account for motion through the image plane. Slice-followed cine DENSE data were acquired to investigate the effects of through-plane motion on the motion-guided segmentation.

A four-channel body phased array RF coil was used. The cine DENSE sequence employed phase cycling to suppress an artifact-generating echo and to improve the SNR by signal averaging (Kim et al., 2004). A series of reference images were also acquired to compensate for phase shifts due to background magnetic field inhomogeneities. A flyback echo planar imaging (EPI) readout was used and DENSE magnitude and phase images were reconstructed online. Imaging parameters included FOV = 360×236 mm; echo train length (ETL) = 9; effective TE = 11 ms; TR = 22 ms; matrix size = 128×94 pixels; voxel size = $2.81 \times 2.81 \times$

8 mm; and displacement encoding frequency $k_e = 0.1$ cycles/mm. The temporal resolution was 44 ms and the number of cardiac phases varied between 15 and 22. Scans were acquired in breath holds of 16 heart beats per encoding direction. Both mid-ventricular short-axis and long-axis views were acquired. Images were analyzed off-line using custom software written in MATLAB (The Mathworks Inc, Natick, MA).

For each dataset, epicardial and endocardial contours were manually drawn at all cardiac phases by an individual with experience in cardiac MRI. Endocardial contours excluded the papillary muscles. Starting points at t_0 were defined using these manually-drawn borders at a single cardiac phase. To quantify the segmentation accuracy and the effect of through-plane motion, distance measurements were made between the manual and motion-guided contours. As shown in Fig 7, these measurements were made radially in the middle of six short axis segments along lines stemming from the centroid of the epicardial contour.

Longitudinal motion of the heart causes the larger-diameter base to move through the short-axis plane during systole. Thus, base-to-apex motion could introduce errors in the short-axis motion guided contours for conventional cine DENSE. Both epicardial and endocardial motion-guided contours could shrink due to through-plane motion during systole and expand due to through-plane motion during diastole when compared to the respective borders on the DENSE magnitude images. To minimize this error, mid-systolic manual contours were used as the initial contours.

To investigate inter-observer error a second observer with experience in cardiac MRI outlined epicardial and endocardial contours on four of the datasets. The automatic contours were compared to manually-drawn contours from both observers using the mean of false positive and false negative area measures. For each observer, the manual contours at mid-systole were used to initiate the motion-guided segmentation process. The false negative area measure identifies the percentage of myocardium missed by the algorithm, and the false positive area measure identifies the percentage of tissue falsely identified by the algorithm. If C_M is the region enclosed by the manually-drawn contour and C_A is the region enclosed by the algorithm's contour, then the false negative area measure is given by $(C_A - (C_M \cap C_A))/C_M$, where $\cap$ denotes intersection. The false positive error is given by $(C_M - (C_M \cap C_A))/C_M$,

5 RESULTS

Fig 8(b) shows a typical early-systolic slice-followed cine DENSE magnitude image with a manually-drawn set of contours. The papillary muscles were excluded from the region identified as LV myocardium. Fig 8(a), (c) and (d) depict the corresponding motion-guided contours for a few cardiac phases. Note in Fig 8(a) that contours are reliably projected onto the first cardiac phase, where many of the borders are indistinguishable to the human observer due to the signal from LV and RV blood.

Based on the mean of false positive and false negative area measures with manually-defined contours for four of the datasets, the segmentation error between the two observers is 18.12 ±5.98%, between observer A and the algorithm is 12.70±4.77%, and between observer B and the algorithm is 11.80±4.12%. This demonstrates that the accuracy of the algorithm relative to manually-drawn contours can be superior to inter-observer variability. The mean and standard deviation of the radial segmentation error for all frames of the 6 slice-followed and 6 conventional cine DENSE datasets are presented in Table 1. There is no noticeable regional error trend. Furthermore, except for the first two frames where the myocardial borders are visually indiscernible due to high blood signal, the errors did not noticeably vary with time. The total average epicardial segmentation error is 0.36±0.08 and 0.40±0.10 pixels (1.01±0.23 and 1.12±0.28 mm) for slice followed and conventional cine DENSE, respectively. The total

average endocardial segmentation error is 0.46±0.12 and 0.46±0.16 pixels (1.29±0.34 and 1.29±0.45 mm) for slice following and conventional cine DENSE, respectively. Note that these error values are specific to short-axis mid-ventricular cine DENSE data, and that although the segmentation error for conventional cine DENSE is slightly greater than for slice-followed cine DENSE for the epicardium, motion-guided segmentation using conventional cine DENSE typically yields very good results. Incorrect phase unwrapping caused the algorithm to fail in 3 out of the total 414 frames (0.72 %). Using a radial segmentation error greater than half a pixel, the segmentation reliability for slice-followed and conventional cine DENSE of a short-axis mid-ventricular view is 90.8 % and 81.6 %, respectively. Using a radial segmentation error greater than one pixel results in a corresponding reliability of 98.8 % and 99.0%. The mean segmentation processing time per frame was 2.4 seconds on a 2.8 GHz Intel Celeron with 256MB of RAM, whereas an experienced user would manually contour the epicardium and endocardium of a single frame in about 30 seconds,

No evidence of errors due to through-plane motion is present in Fig 8 and evidence of this effect is minimal in Table 1. Fig 9 gives an extreme example of the effect of through-plane motion when the segmentation algorithm is applied to conventional cine DENSE data. Fig 9 (a) and (b) depict the swelling and shrinking of the motion-guided contours that accompanies diastole and systole, respectively. The effect was exaggerated here by drawing the manual contour at end-systole for Fig 9(a), and at late-diastole for Fig 9(b).

To further demonstrate the flexibility of the method, the algorithm was applied to a set of long-axis conventional cine DENSE images. Figure 10 shows the results of this process, where Figure 10(c) is the manually drawn contour, and the remaining images portray the mapping of this contour onto preceding and successive frames. Due to the shape of the LV in the long-axis view, periodic Fourier functions were not used to smooth the contours. Whereas the periodic Fourier fits presented here are all well-suited for short-axis contours where the LV is shaped like a torus, periodic splines may be a more suitable alternative for long-axis images or arbitrary regions of myocardium.

6 DISCUSSION

Both cine DENSE and velocity-encoded PC have the potential to incorporate information from magnitude and phase images to assist the segmentation process. Although velocity-encoded magnitude images are not interrupted by tag lines, they are "white blood" sequences and thus suffer from a lack of contrast between blood and myocardium. Wong et al. (2002) presented a myocardial segmentation technique where velocity fields from velocity-encoded were combined with a two-stage front propagation technique. Velocity information was incorporated based on the front distribution at the preceding cardiac phase. Although only initial qualitative results were presented, it is clear that the velocity constrained contours for both the epi- and endocardium were superior to those obtained using intensity information alone. In a related study, Cho and Benkeser (2006) proposed a velocity-aided cardiac segmentation method for the endocardium based on a modified active contour model. They introduced a new image force called the tensor-based orientation gradient force and a significant improvement was seen when the orientation gradient force was taken into account. Although the segmentation algorithm presented here is based entirely on the cine DENSE phase images, there could be benefit in incorporating edge information from the magnitude images. More specifically, there is potential for completely automating the cine DENSE segmentation by using edge information to define the initial contours or region of interest.

Some early attempts to automate contour detection for tagged images made use of manually-guided active geometry (Kumar and Goldgof, 1994; Young et al., 1995; Kraichman et al., 1995). Guttman et al. (1994) presented a completely automated approach that performed well

for detection of the endocardial boundary in both short- and long-axis images, but limited manual correction was sometimes required for the epicardium. Montillo et al. (2002) developed a completely automated feature-based method that uses volumetric data of stacked short-axis tagged images. Montillo et al. (2003) furthered this work and developed an automated, deformable model-based method to segment the left and right ventricles in 4D tagged MR. The work presented here brings the level of automation in cine DENSE processing closer to the level of automation already achieved by other researchers for tagged MRI. If 3D cine DENSE data are acquired (Gilson et al., 2005; Moghaddam et al., 2006; Zhong et al., 2007:3) then this single slice segmentation algorithm could be extended to 3D, where a predefined volume of myocardium would be projected through time onto other cardiac phases using the measured 3D motion trajectories. The method could be completely automated by incorporating the additional edge information available from the 3D cine DENSE magnitude images and possibly using a deformable surface model. A comprehensive review of 3D models for functional analysis of cardiac images is given in Frangi et al. (2001).

The cine DENSE strain maps portray realistic strain values and we thus do not suspect negative Jacobian determinants in the deformation field. The heuristic rules also should serve to avoid negative Jacobian determinants. For propagating the endocardial and epicardial contours, the trajectories near the boundary are more important than those near the midwall. Computational effort could be significantly reduced by tracking only a ring of points near the epi- and endocardial boundaries. Contours could then be fitted through these points at all frames and modified to meet the myocardial borders by inflating the epicardial contours by a half-pixel radius and deflating the endocardial contours by a half-pixel radius. Further work is required to implement and validate this approach.

Given that the segmentation accuracy is comparable to inter-observer variability, it can be argued that the algorithm will sometimes produce more accurate contours than a trained user. In particular, whereas it may be difficult for a user to consistently identify the same portion of myocardium for each cardiac phase, the segmentation algorithm inherently only includes related myocardial displacement vectors that contribute to the tissue tracking. The error values in Table 1 show no obvious regional relationship to the six radial segments. In particular, although we expected the errors in the free wall to be greater than those in the septum, no such relationship is evident. This is likely because the errors due to though-plane motion are less than the observer variability. The presence of papillary muscles complicates the placement of manual contours which may explain why the errors for the endocardium are generally greater than those for the epicardium. An increase in segmentation error with time was also expected due to the T1-related decay in SNR that is characteristic of cine DENSE images. No temporal component to the error is evident which again implies that this error variability is less than the observer variability. An exception to this is the first few frames where high signal is present in the blood and endocardial contours are visually indistinguishable. Gauging by the general performance of the segmentation technique, the motion-guided endocardial contours are probably more accurate than the manual contours for the first few frames.

There are a number of advantages to the cine DENSE motion-guided segmentation method described here: 1. the parameters used to discern between useful and noisy vectors are all based on practical physiological limits; 2. contours are calculated for the first few cardiac phases, where it is difficult to visually distinguish blood from myocardium; 3. whereas many segmentation methods are specific to a particular view of the heart, this motion-guided segmentation is independent of the imaging plane; and 4. the method is independent of the shape of the tissue delineated, and any arbitrary portions of the myocardium can be tracked through time.

The method also has several limitations and possible sources of error. An assumption underlying the method is that the measurement of the myocardial displacement field is fairly accurate. If this is not the case, then not only will the segmentation be poor, but the measured cardiac strain field will also be erroneous. However, cine DENSE phantom studies measuring both displacement (Spottiswoode et al., 2007) and strain (Hettiwatte et al., 2007) strongly support the assumption of accuracy. Possible sources of segmentation error include those introduced by the user in the initially-defined contour and image misregistration between the two breath holds. Errors introduced by poorly-drawn initial contours will generally be propagated onto the contours of all other frames. A further potentially limiting factor, particularly for thin myocardial walls, is the reduced accuracy in the displacement measurements due to partial volume effects near the myocardial borders. In the event that the myocardial thickness spans only a pixel or two, it is possible for discontinuities to exist in the perceived myocardial walls. Although no such discontinuities arose for the data used in this study, active contour models (Kass et al., 1988) could be adapted to bridge these gaps, but this is a nontrivial task and the implementation would differ considerably in short and long axis views. Finally, the present technique has only been thoroughly validated in a mid-ventricular short axis view of the heart and further work is required to evaluate the method throughout the rest of the heart.

As is apparent when comparing Fig 8 with Fig 9, the SNR of slice followed cine DENSE is lower than the SNR of conventional cine DENSE. The SNR can be increased significantly using a spiral readout (Zhong et al., 2007:2). Furthermore, phase SNR can be increased using balanced multipoint encoding (Zhong et al., 2007:1). Finally, a field strength of 3T may improve SNR for cine DENSE, however this has yet to be thoroughly investigated.

The concept of motion-guided segmentation using tissue tracking also has potential value in areas beyond cine DENSE. It could, for example, be used in ultrasound speckle tracking, where the correlated speckle pattern is tracked from frame-to-frame through the cardiac cycle using block matching (Li et al., 2006). The idea of using phase-based tracking to extrapolate myocardial contours through time has been presented previously for harmonic phase (HARP) analysis by Osman et al. (1999). HARP is analogous to DENSE in many ways (Kuijer et al., 2006), and the existence of several HARP tissue tracking techniques (Osman et al., 1999; Pan et al., 2003, 2005; Abd-Elmoniem et al., 2005, 2006) encourages further development for motion-guided segmentation in HARP.

7 CONCLUSION

A reliable and effective 2D segmentation method has been developed for 2D cine DENSE, where encoded myocardial motion is used to project a set of contours through time. The total user interaction in cine DENSE image analysis is thus reduced to the manual demarcation of the myocardium on a single frame. The technique is solely based on the cine DENSE phase images, but the additional use of magnitude information holds promise for further automation. A radial segmentation error metric was introduced for short-axis data, and results are presented for 6 slice-followed and 6 non slice-followed datasets. The total average epicardial segmentation error is 0.36 ± 0.08 and 0.40 ± 0.10 pixels (1.01 ± 0.23 and 1.12 ± 0.28 mm) for slice following and conventional cine DENSE, respectively. The total average endocardial segmentation error is 0.46 ± 0.12 and 0.46 ± 0.16 pixels (1.29 ± 0.34 and 1.29 ± 0.45 mm) for slice followed and conventional cine DENSE, respectively. The segmentation accuracy is similar to inter-observer variability. Motion-guided segmentation can be accurately achieved by employing the displacement-encoded phase shifts intrinsic to cine DENSE MRI to propagate a single set of predefined contours throughout the remaining cardiac phases.

Supplementary Material

Refer to Web version on PubMed Central for supplementary material.

Acknowledgements

References

Abd-Elmoniem, KZ.; Osman, NF.; Prince, JL.; Stuber, M. zHARP: 3-D cardiac motion tracking from short-axis acquisitions. Proceedings of the 13th International Society for Magnetic Resonance in Medicine (ISMRM); 2005. p. 1649

Abd-Elmoniem, KZ.; Stuber, M.; Prince, JL. Fast 3D dense tracking of cardiac material points using ZHARP: in-vivo validation and comparison with 3D SF-HARP. Proceedings of the 14th International Society for Magnetic Resonance in Medicine (ISMRM); 2006. p. 1653

Aletras A, Ding S, Balaban R, Wen H. DENSE: displacement encoding with stimulated echoes in cardiac functional MRI. Journal of Magnetic Resonance 1999;137:247–252. [PubMed: 10053155]

Axel L, Dougherty L. MR imaging of motion with spatial modulation of magnetization. Radiology 1989;171:841–845. [PubMed: 2717762]

Bryant D, Payne J, Firmin D, Longmore D. Measurement of flow with NMR imaging using gradient pulse and phase difference technique. Journal of computer assisted tomography 1984;8(4):588–593. [PubMed: 6736356]

Cho J, Benkeser PJ. Cardiac segmentation by a velocity-aided active contour model. Computerized Medical Imaging and Graphics 2006;30:31–41. [PubMed: 16378714]

Fischer S, McKinnon G, Maier S, Boesiger P. Improved myocardial tagging contrast. Magnetic Resonance in Medicine 1993;30:191–200. [PubMed: 8366800]

Fischer SE, McKinnon GC, Scheidegger MC, Prins W, Meier D, Boesiger P. True myocardial motion tracking. Magnetic Resonance in Medicine 1994;31:401–413. [PubMed: 8208116]

Frangi AF, Niessen WJ, Viergever MA. Three-dimensional modelling for functional analysis of cardiac images: A review. IEEE Transactions on Medical Imaging 2001;20(1):2–25. [PubMed: 11293688]

Gilson WD, Yang Z, French BA, Epstein FH. Measurement of myocardial mechanics in mice before and after infarction using multislice displacement-encoded MRI with 3D motion encoding. American Journal of Physiology – Heart and Circulatory Physiology 2005;288(3):H1491–H1497. [PubMed: 15513963]

Gotte MJ, van Rossum AC, Twisk JWR, Kuijer JPA, Marcus JT, Visser CA, et al. Quantification of regional contractile function after infarction: strain analysis superior to wall thickening analysis in discriminating infarct from remote myocardium. Journal of the American College of Cardiology 2001;37(3):808–817. [PubMed: 11693756]

Guttmann MA, Prince JL, McVeigh ER. Tag and contour detection in tagged MR images of the left ventricle. IEEE Transactions on Medical Imaging 1994;13(1):74–88. [PubMed: 18218485]

Hettiwatte SN, Kirton RS, Kuijer JPA, Epstein FH, Cowan BR, Young AA. Comparison of SPAMM, HARP, and DENSE in a Deformable Phantom. Journal of Cardiovascular Magnetic Resonance 2007;9(2):505.

Kass M, Witkin A, Terzopoulos D. Snakes: Active contour models. International Journal of Computer Vision 1988;1:321–331.

Kim D, Gilson W, Kramer C, Epstein F. Myocardial tissue tracking with two-dimensional cine displacement-encoded MR imaging: Development and initial evaluation. Radiology 2004;230:862–871. [PubMed: 14739307]

Kuijer, J.; Hofman, MB.; Zwanenburg, JJ.; Marcus, JT.; Rossum, AC.; Heethaar, RM. DENSE and HARP: two views on the same technique of phase-based strain imaging. Proceedings of the 14th International Society for Magnetic Resonance in Medicine (ISMRM); 2006.

Kumar S, Goldgof D. Automatic tracking of SPAMM grid and the estimation of deformation parameters from cardiac MR images. IEEE Transactions on Medical Imaging 1994;13(1):122–132. [PubMed: 18218489]

Li, Y.; Garson, CD.; Epstein, FH.; French, BA.; Hossack, JA. High resolution 2–D quantification of myocardial motion abnormalities in mice using high resolution ultrasound with MRI validation. Proceedings of the 3rd International Symposium on Biomedical Engineering (ISBI); 2006.

Moghaddam, AN.; Wen, H.; Gharib, M. More comprehensive cardiac DENSE MR imaging by combination of short axis and long axis data. Proceedings of the 14th International Society for Magnetic Resonance in Medicine (ISMRM); 2006. p. 1652

Moore CC, Lugo-Olivieri CH, McVeigh ER, Zerhouni EA. Three dimensional systolic patterns in the normal human left ventricle: characterization with tagged MR imaging. Radiology 2000;214:453–466. [PubMed: 10671594]

Montillo A, Metaxas D, Axel L. Automated segmentation of the left and right ventricles in 4–D cardiac SPAMM images. International Society and Conference Series on Medical Image Computing and Computer-Assisted Intervention (MICCAI), LNCS 2002;2488:620–633.

Montillo A, Metaxas D, Axel L. Automated model-based segmentation of the left and right ventricles in tagged cardiac MRI. International Society and Conference Series on Medical Image Computing and Computer-Assisted Intervention (MICCAI), LNCS Vol 2003;2878:507–515.

Osman NF, Kerwin WS, McVeigh ER, Prince JL. Cardiac motion tracking using CINE harmonic phase (HARP) magnetic resonance imaging. Magnetic Resonance in Medicine 1999;42:1048–1060. [PubMed: 10571926]

Osman NF, McVeigh ER, Prince JL. Imaging Heart Motion Using Harmonic Phase MRI. IEEE Transactions on Medical Imaging 2000;19(3):186–202. [PubMed: 10875703]

Pan L, Lima JAC, Osman NF. Fast tracking of cardiac motion using 3DHARP. Proceedings of Information Processing and Medical Imaging (IPMI), LNCS 2003;2732:611–622.

Pan, L.; Sampath, S.; Prince, JL.; Stuber, M.; Osman, NF. Fast tracking of cardiac material points from SF-CSPAMM images using 3D SF-HARP. Proceedings of the 13th International Society for Magnetic Resonance in Medicine (ISMRM); 2005.

Spottiswoode BS, Zhong X, Lorenz CH, Meintjes EM, Mayosi BM, Epstein FH. 3D Myocardial Tissue Tracking with Slice Followed Cine DENSE MRI. Journal of Magnetic Resonance Imaging. 2008in press

Spottiswoode BS, Zhong X, Hess AT, Kramer CM, Meintjes EM, Mayosi BM, Epstein FH. Tracking Myocardial Motion from Cine DENSE Images using Spatiotemporal Phase Unwrapping and Temporal Fitting. IEEE Transactions on Medical Imaging 2007;26(1):15–30. [PubMed: 17243581]

Stuber M, Spiegel MA, Fischer SE, Scheidegger MB, Danias PG, Pedersen EM, Boesiger P. Single breath-hold slice-followed CSPAMM myocardial tagging. Magnetic Resonance Materials in Physics, Biology and Medicine 1999;9:85–91.

van Dijk P. Direct cardiac MNR imaging of heart wall and blood flow velocity. Journal of computer assisted tomography 1984;8(3):429–436. [PubMed: 6725689]

Wong, ALN.; Liu, H.; Shi, P. Segmentation of the Myocardium Using Velocity Field Constrained Front Propagation. Proceedings of the 6th IEEE Workshop on Applications of Computer Vision; 2002. p. 84

Young AA, Kraitchman DL, Dougherty L, Axel L. Tracking and finite element analysis of stripe deformation in magnetic resonance tagging. IEEE Transactions on Medical Imaging 1995;14(3): 413–421. [PubMed: 18215845]

Zerhouni EA, Parish DM, Rogers WJ, Yang A, Shapiro EP. Human heart: tagging with MR imaging – a method for noninvasive assessment of myocardial motion. Radiology 1988;163(1):59–63. [PubMed: 3420283]

Zhong, X.; Helm, P.; Young, A.; Kirton, R.; Epstein, FH. 1. Improved DENSE MRI Using Balanced Multi-point Displacement Encoding. Proceedings of the 15th International Society for Magnetic Resonance in Medicine (ISMRM); 2007. p. 965

Zhong, X.; Spottiswoode, BS.; Meyer, CH.; Epstein, FH. 2. Two-dimensional Spiral Cine DENSE. Proceedings of the 15th International Society for Magnetic Resonance in Medicine (ISMRM); 2007. p. 756

Zhong, X.; Spottiswoode, BS.; Epstein, FH. 3. Myocardial Tissue Tracking Using Volumetric Cine DENSE with Three-dimensional Displacement Encoding: Development and Preliminary Results. Proceedings of the 15th International Society for Magnetic Resonance in Medicine (ISMRM); 2007. p. 3599
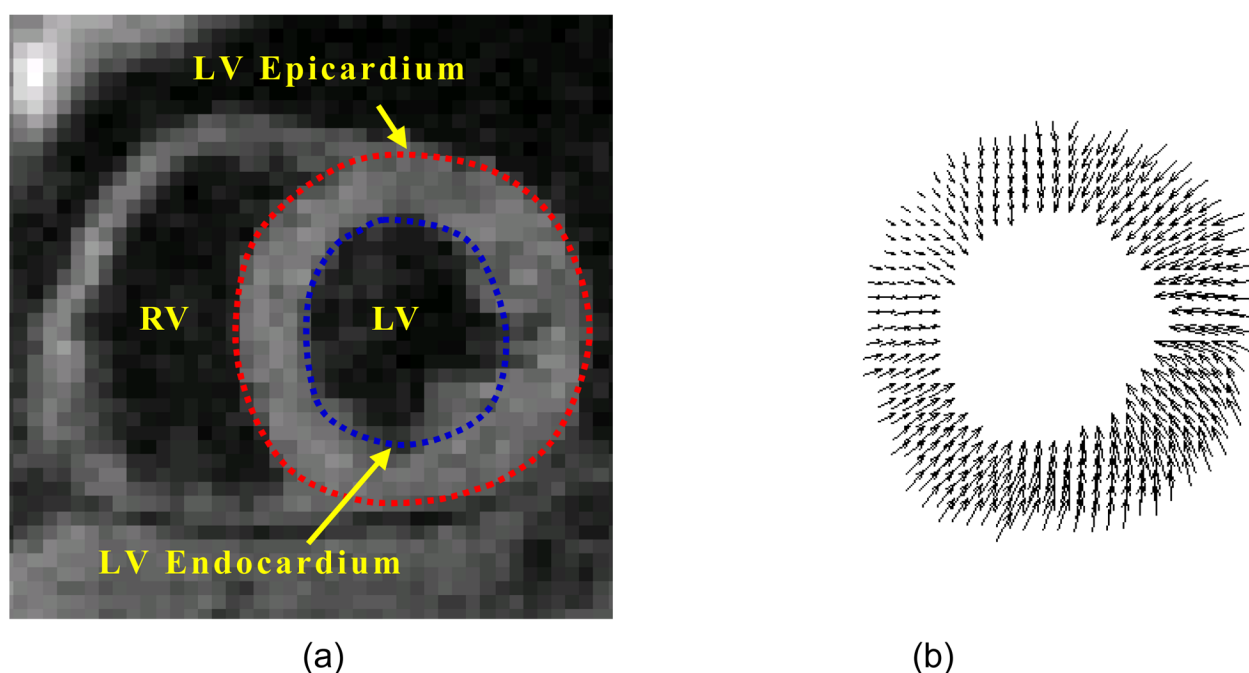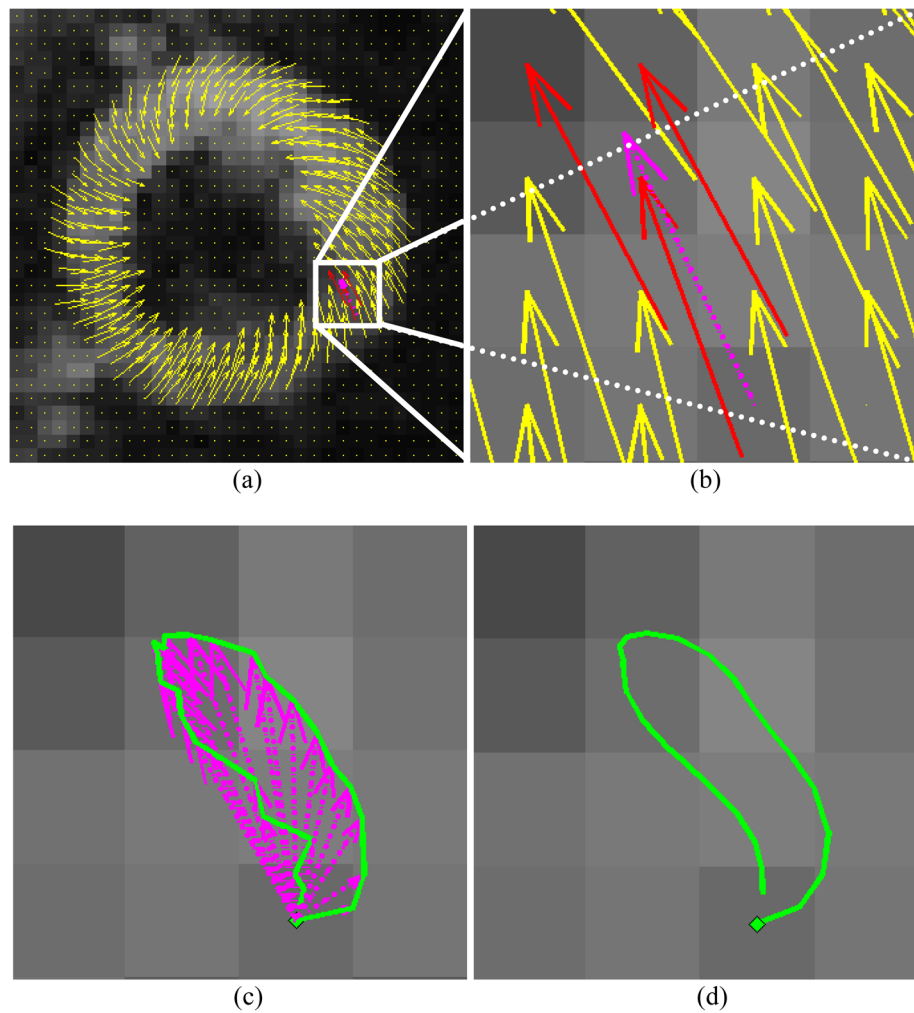
(a)   (b)

Fig 1.
(a) Cine DENSE magnitude mid-ventricular short-axis view of the heart at end-systole. LV –
left ventricle; RV –right ventricle. (b) Two dimensional in-plane displacement field derived
from the corresponding vertically and horizontally encoded unwrapped cine DENSE phase-
reconstructed images.

Fig 2.
Cine DENSE 2D tissue tracking. (a) End-systolic DENSE displacement field. (b) Magnified portion of this displacement field. The tail of the dotted (purple) vector corresponds to the chosen material point to be tracked from t_0. The three solid dark (red) vectors are the vectors at this frame used for the interpolation, and the dotted vector is the interpolated vector. (c) A frame-to-frame trajectory is obtained by subtracting the interpolated vectors of successive frames. (d) The improvement that results from fitting 5th order Fourier basis functions to motion trajectories in $\hat{\imath}$ and $\hat{\jmath}$ directions.
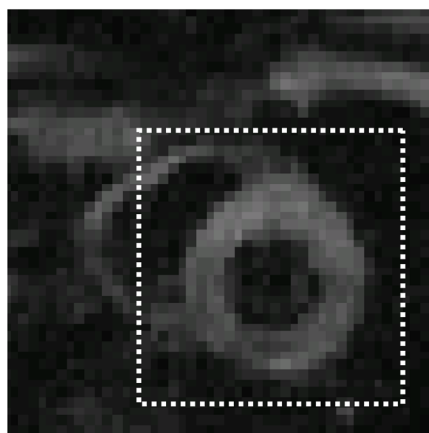
(a)
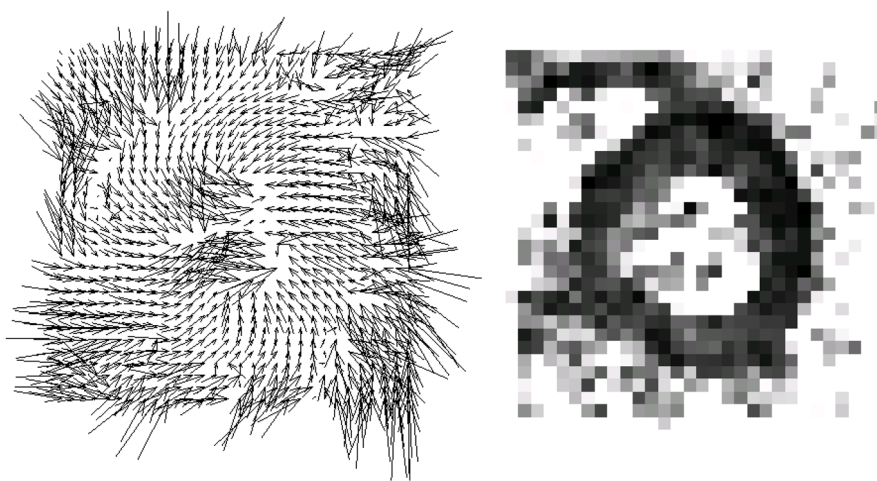
Fig 3.
(a) Magnitude-reconstructed overview image, (b) corresponding DENSE displacement field derived by applying spatiotemporal phase unwrapping without pre-defined contours, and (c) the corresponding deformation mask.
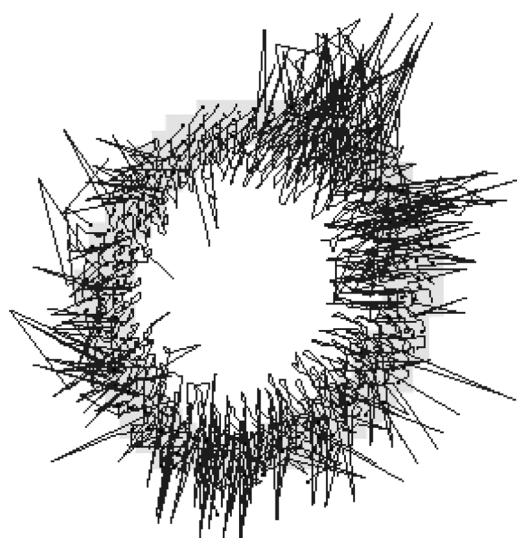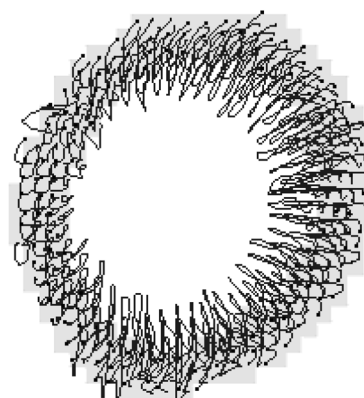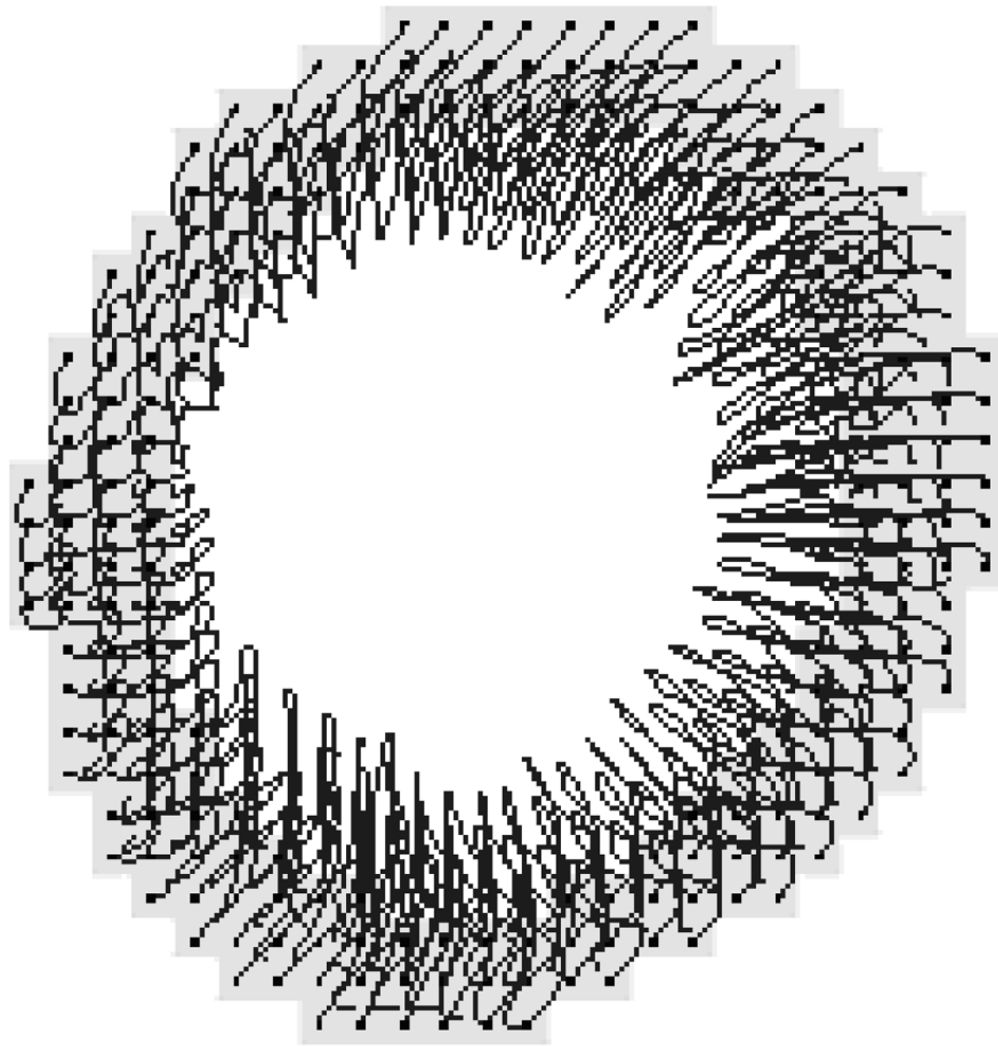
(a)
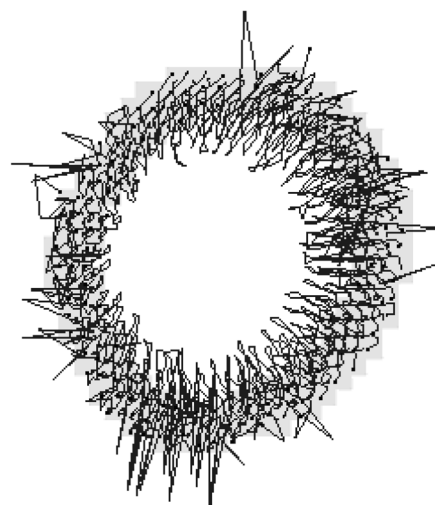
(b)
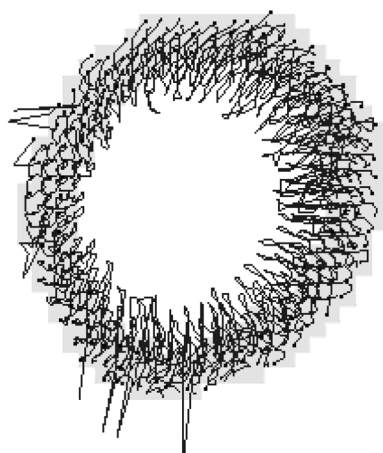
(c)

(d)

(e)

Fig 4.
(a) Frame-to-frame trajectories obtained by tracking using the 3 closest vector tails, (b) frame-to-frame trajectories after applying the deformation mask, (c) frame-to-frame trajectories after applying both the deformation mask and the heuristic vector magnitude and angle deviation criteria, and (d) frame-to-frame trajectories after applying all of the above criteria plus temporal fitting with 5th order Fourier basis functions. (e) Frame-to-frame trajectories obtained if the displacement data is masked using the motion-guided contours and if the trajectories commence from the centers of a uniform grid of pixels in the first frame.
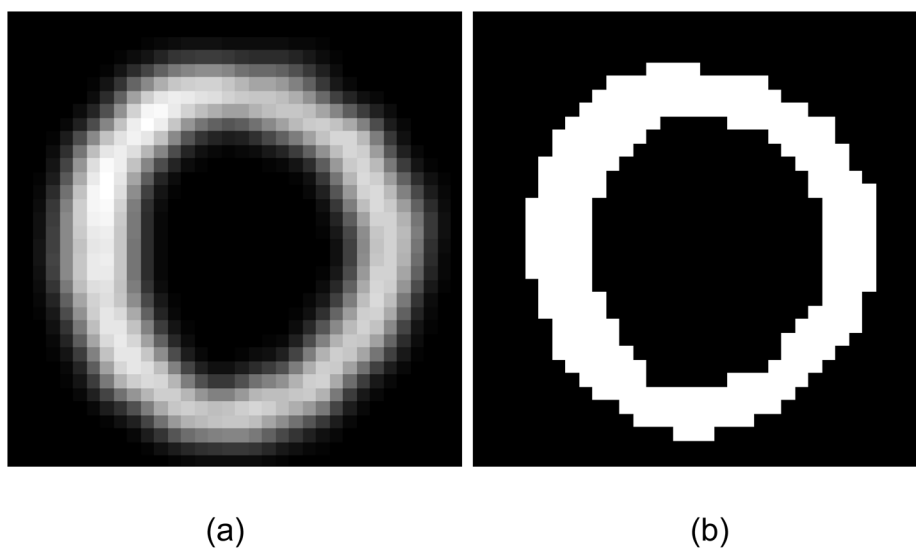
(a) (b)

Fig 5.
(a) Smooth myocardial image obtained by representing each trajectory position at the current frame by a 2D Gaussian function with an area of unity and a standard deviation of 1.25 pixels. (b) Applying a threshold of 0.5 to the smooth myocardial image gives a pixilated binary mask of the myocardium.
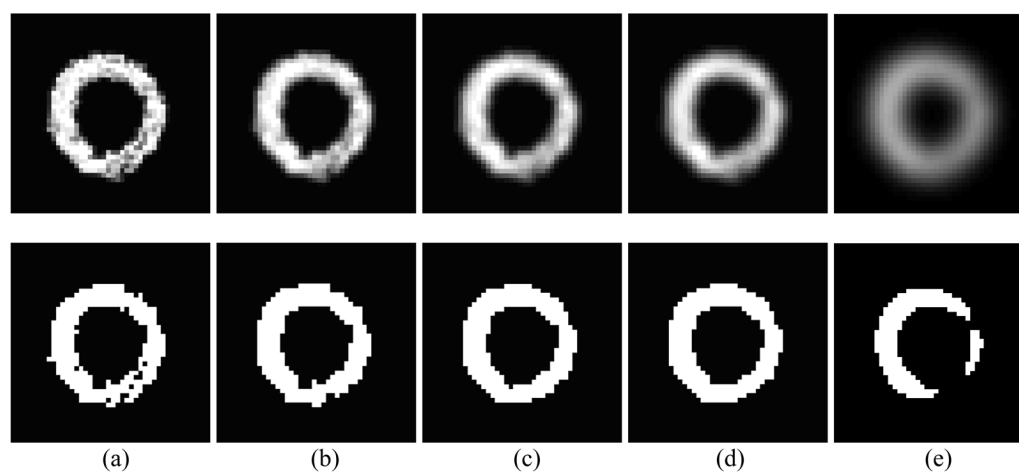
(a)   (b)   (c)   (d)   (e)

Fig 6.
Smooth (top) and thresholded (bottom) images of the myocardium for a single frame with varying values of the Gaussian standard deviation σ. (a) σ=0.5, (b) σ=0.75, (c) σ=1, (d) σ=1.25, and (e) σ=2.75. Inconsistencies are apparent in (a) and (e).
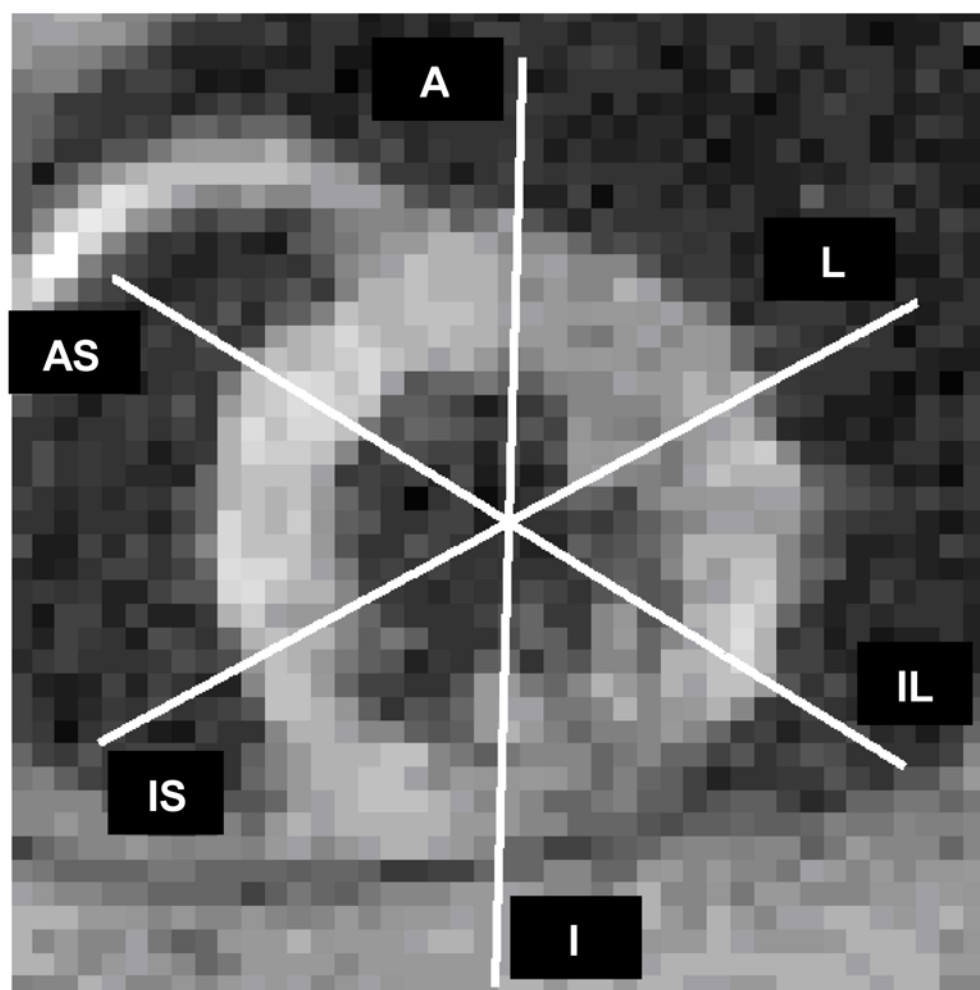
Fig 7.
Short-axis view of the heart showing the six radial spokes along which differences between manual and automated contours are measured. A – anterior; L – lateral; IL – inferolateral; I – inferior; IS – inferior septum; AS –anterior septum. Each line corresponds to the centre of the corresponding short axis segment.
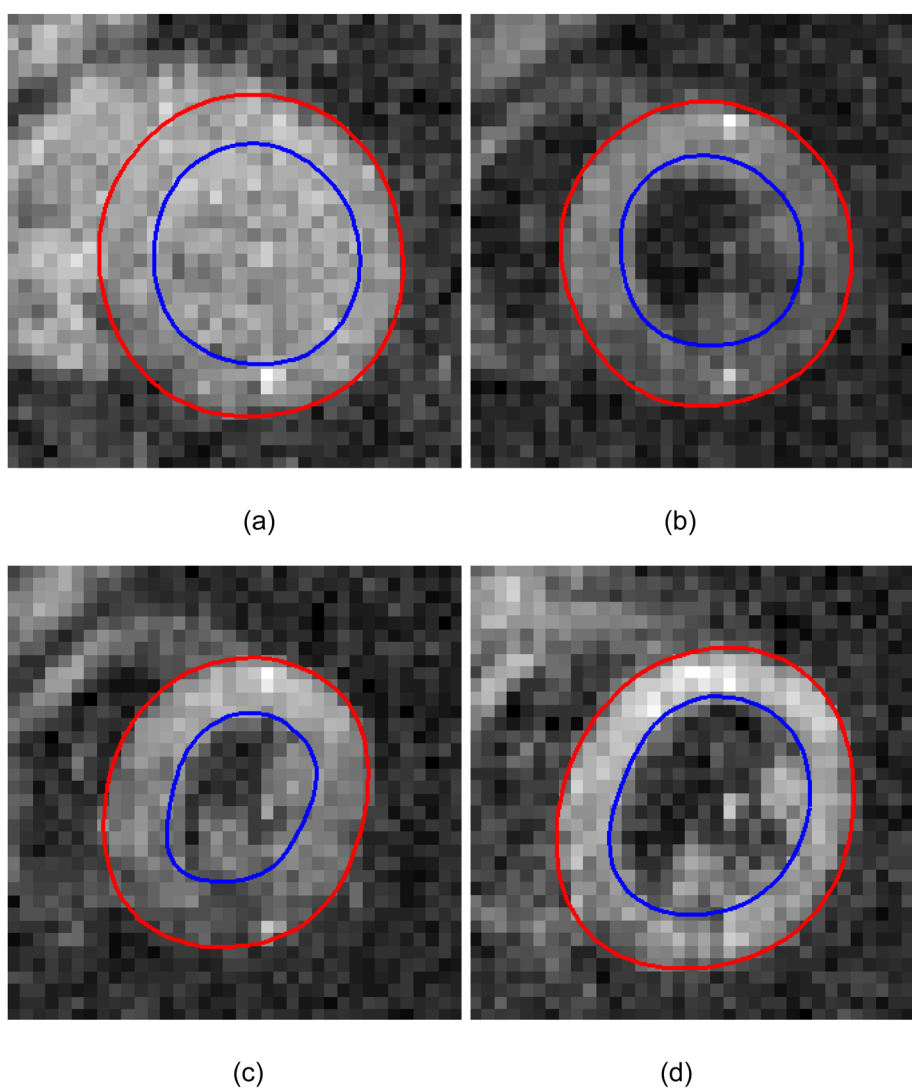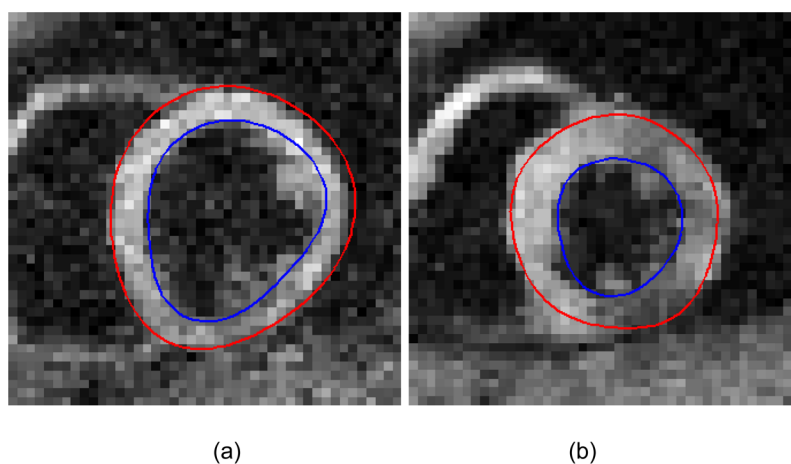
Fig 8.
Magnitude-reconstructed slice followed cine DENSE images of a short-axis view at (a) end-diastole, (b) early-systole, (c) end-systole, and (d) mid-diastole. The manually-drawn contour is shown in (b) and the corresponding motion-guided contours are shown in (a), (c), and (d).

(a)   (b)

Fig 9.
Effect of through-plane motion on motion-guided segmentation in conventional cine DENSE data of a mid-ventricular short-axis slice of a normal volunteer. (a) Motion-guided contour at late-diastole, where the manually defined contour was drawn at end-systole. (b) Motion-guided contour at end-systole, where the manually defined contour was drawn at late-diastole.
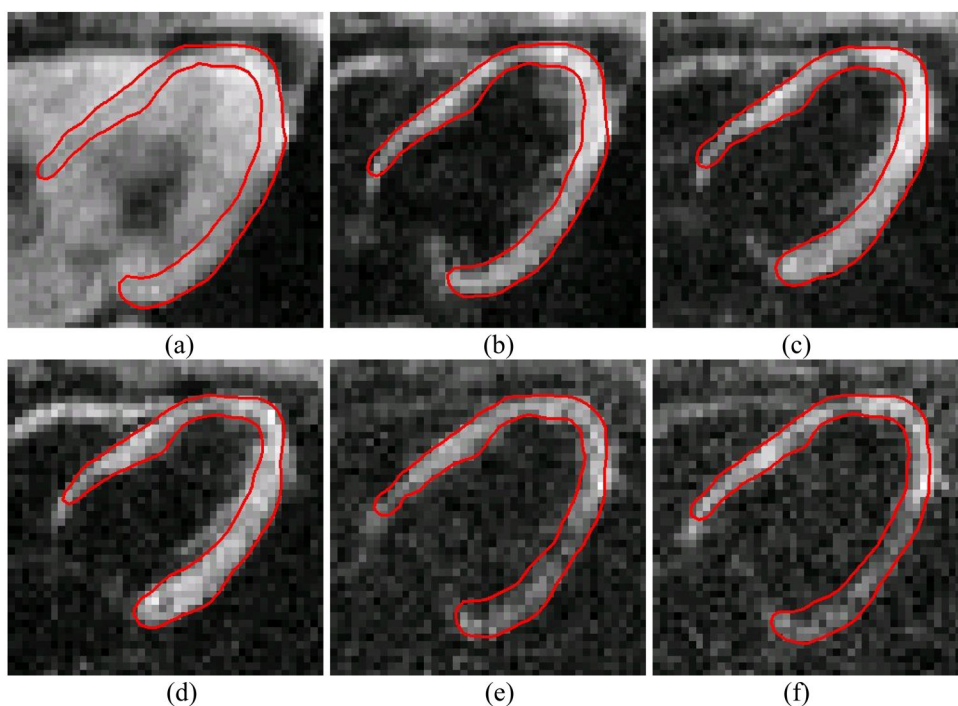
Fig 10.
Motion-guided segmentation applied to long-axis conventional cine DENSE data. (a) End-diastole, (b) early-systole, (c) mid-systole, (d) end-systole, (e) mid-diastole, and (f) late-diastole. The manual contour was drawn at mid-systole.

Table 1

Regional mid ventricular short-axis radial segmentation error and standard deviation (in pixels) measured by comparing manual and motion-guided contours. A – anterior; L – lateral; IL – inferolateral; I – inferior; IS – inferior septum; AS – anterior septum. The pixel size was 2.81×2.81 mm^2.

		A	L	IL	I	IS	AS
Epicardium	Non slice followed	0.37±0.05	0.43±0.13	0.38±0.06	0.37±0.09	0.46±0.12	0.40±0.11
	Slice followed	0.34±0.08	0.35±0.06	0.39±0.11	0.38±0.09	0.30±0.04	0.40±0.05
Endocardium	Non slice followed	0.48±0.22	0.58±0.24	0.39±0.11	0.48±0.07	0.46±0.14	0.36±0.11
	Slice followed	0.53±0.21	0.44±0.08	0.48±0.16	0.47±0.12	0.43±0.08	0.39±0.03

Table A1

A list of the free parameters and their effect on the motion-guided segmentation algorithm and the selection criteria.

Parameter	Value	Increase	Decrease	Set by
Magnitude deviation	0.7	Fewer noisy vectors removed	More noisy vectors removed	Cardiac strain limits
Angle deviation	pi/6	Fewer noisy vectors removed	More noisy vectors removed	Experience with DENSE displacement vectors at a 2.81×2.81 mm^2 spatial resolution
Deformation mask threshold	0.7	Fewer noisy vectors removed	More noisy vectors removed	Cardiac strain limits
Gaussian standard deviation	1.25	Smoother image but large islands of myocardium may appear	Less smooth image but small islands of non-myocardium may appear	Kept as small as possible but large enough to give a smooth image. See Fig 6.
Fourier fit order	4	Less contour smoothing	Greater contour smoothing	The LV contours (excluding papillary muscles) are relatively simple in shape. The fit order was made just large enough to accommodate reasonable variations in this shape.